Am J Transl Res 2026;18(5):4356-4372
www.ajtr.org /ISSN:1943-8141/AJTR0172342

Original Article

Low-dose CT for assessing microstructural alterations in Renal Osteodystrophy among uremic patients: a retrospective cohort study

Hui Liu[1], Huihua Wang[2], Chenhong Liu[1], Huapeng Xie[1], Lijun Xiang[1], Rencong Xu[3]

[1]Department of Radiology, Affiliated Hospital of Jinggangshan University, Ji'an 343400, Jiangxi, China; [2]Clinical Medical Research Center, Affiliated Hospital of Jinggangshan University, Ji'an 343400, Jiangxi, China; [3]Department of Nephrology, Ganzhou People's Hospital, Ganzhou 341000, Jiangxi, China

Received February 28, 2026; Accepted April 13, 2026; Epub May 15, 2026; Published May 30, 2026

Abstract: Background: Renal Osteodystrophy (ROD) is a severe complication among uremic patients. However, the gold standard for diagnosis, bone biopsy, is invasive and difficult to apply routinely. Although low-dose CT (LDCT) is widely used for other assessments in this population, its value in the non-invasive diagnosis of ROD remains to be elucidated. Purpose: To investigate the feasibility and diagnostic performance of quantitative assessment of lumbar vertebral microstructural changes using routine LDCT images for the identification and diagnosis of ROD and its subtypes. Methods: This was a retrospective cohort study. A total of 155 uremic patients undergoing regular dialysis who concurrently underwent abdominal/pelvic LDCT and bone metabolic biochemical tests at the Affiliated Hospital of Jinggangshan University between June 2023 and June 2025 were consecutively enrolled. Based on the KDIGO guidelines combined with biochemical markers (iPTH, calcium, phosphorus, ALP, etc.), patients were categorized into a non-ROD group (n = 49), high-turnover ROD (n = 44), low-turnover ROD (n = 30), and mixed-type ROD (n = 32). Using 3D Slicer software, the following parameters were measured in the trabecular bone region of the L1/L2 vertebral bodies: volumetric bone mineral density (vBMD), bone volume fraction (BV/TV), trabecular thickness (Tb.Th), trabecular separation (Tb.Sp), trabecular number (Tb.N), and cortical thickness (Ct.Th). Inter-group differences were compared, correlations between CT parameters and biochemical markers were analyzed, and the diagnostic performance was evaluated using Receiver Operating Characteristic (ROC) curves. Results: The overall prevalence of ROD was 68.4% (106/155). Significant differences in biochemical markers and CT parameters were observed among the ROD subtypes (all P<0.001). High-turnover ROD exhibited the highest iPTH (552.60 ± 115.90 pg/mL), ALP (260.55 ± 50.29 U/L), and the worst bone microstructure (lowest BV/TV: 13.89 ± 3.09%, highest Tb.Sp: 1.03 ± 0.15 mm). Tb.Sp demonstrated the best performance in differentiating ROD from non-ROD, with an Area Under the Curve (AUC) of 0.902 (sensitivity 81.1%, specificity 89.8%, cutoff value 0.84 mm). CT parameters (e.g., BV/TV, vBMD, Tb.Sp) showed significant correlations with iPTH, ALP, and serum phosphorus ($|r|$ = 0.429-0.579, P<0.001). When combining iPTH with BV/TV to construct a model, the diagnostic AUC improved to 0.888. Additionally, bone microstructure parameters showed significant correlations with coronary artery calcification (e.g., BV/TV: r = -0.383, P<0.001), supporting the bone-vascular axis concept. Conclusion: Quantitative analysis of lumbar vertebral microstructure using existing LDCT images in uremic patients can effectively differentiate ROD subtypes and corroborate biochemical changes, with trabecular separation (Tb.Sp) showing outstanding diagnostic value. This method serves as a non-invasive and convenient auxiliary tool that may facilitate the clinical identification and precise management of ROD.

Keywords: Renal Osteodystrophy, tomography, X-ray computed, bone microstructure, diagnosis, uremia

Introduction

Renal Osteodystrophy (ROD) is a common and severe complication of mineral and bone metabolism disorders in patients with chronic kidney disease (CKD), particularly end-stage renal disease (uremia) [1]. Its primary pathological alterations involve abnormalities in bone turnover, mineralization, and volume, with clinical classifications encompassing high-turnover, low-turnover, and mixed types [2]. ROD not only leads to significant bone pain and increased fracture risk but is also closely associated with vascular calcification, cardiovascu-

https://doi.org/10.62347/VGYF3652

lar events, and elevated all-cause mortality, severely impacting patients' quality of life and long-term prognosis [3, 4].

Currently, the "gold standard" for diagnosing and classifying ROD remains as histomorphometric analysis following iliac bone biopsy [5, 6]. However, this technique is invasive, complex to perform, prone to sampling errors, poorly accepted by patients, and difficult to repeat, thereby limiting its widespread application in routine clinical practice and dynamic monitoring [7, 8]. In clinical practice, physicians primarily rely on serum biochemical markers, such as intact parathyroid hormone (iPTH), calcium, phosphorus, and alkaline phosphatase (ALP), for evaluation and classification [9, 10]. Although these markers are indispensable, their correlation with histological bone changes is not entirely consistent. Furthermore, they cannot directly and quantitatively reflect the true state of bone microstructure, potentially leading to underestimation or misjudgment of bone status in some patients [11, 12]. Consequently, there is an urgent clinical need to develop a non-invasive, accurate, and quantitative method for assessing bone microstructure to facilitate the early identification, precise classification, and therapeutic follow-up of ROD.

Recent advances in medical imaging have provided new avenues for non-invasive bone quality assessment. High-resolution peripheral quantitative CT (HR-pQCT) can precisely quantify bone microstructure; however, it suffers from high equipment costs, low availability, and limited scanning range [13]. In contrast, conventional CT, particularly low-dose CT (LDCT), is widely used in the clinical evaluation of uremic patients - for instance, for coronary artery calcium scoring, urolithiasis examination, and diagnosis of primary diseases [14, 15]. These examinations often cover the lumbar spine region. Theoretically, utilizing the grayscale information (Hounsfield Units, HU) from existing CT images and conducting morphological analyses via post-processing software can derive quantitative parameters reflecting bone density and trabecular microstructure, such as bone volume fraction (BV/TV), trabecular separation (Tb.Sp), and trabecular thickness (Tb.Th) [16, 17]. This presents a potential opportunity for "secondary analysis" of routine LDCT images to evaluate ROD. However, systematic evidence regarding the feasibility, diagnostic performance, and correlation with clinical biochemical markers of quantitative bone microstructural parameters derived from conventional LDCT for diagnosing ROD and its subtypes in the Chinese uremic dialysis population remains lacking.

Based on this, the present study aims to investigate the feasibility of quantitatively measuring lumbar spine microstructural parameters using existing abdominal or pelvic low-dose CT (LDCT) images from uremic patients, to non-invasively distinguish Renal Osteodystrophy (ROD) from non-ROD and differentiate among various ROD subtypes through a retrospective cohort analysis. We plan to systematically compare parameter differences among groups, analyze their correlations with serum biochemical markers, and evaluate the diagnostic performance of key parameters via Receiver Operating Characteristic (ROC) curves. Ultimately, we aim to establish a convenient and effective imaging-assisted diagnostic tool, providing new evidence for the precise management of ROD in clinical practice.

Materials and methods

Study design and ethics statement

This study was a single-center, retrospective cohort study. The study protocol was approved by the Institutional Review Board/Ethics Committee of Affiliated Hospital of Jinggangshan University. All procedures were conducted in accordance with the principles of the Declaration of Helsinki (2013 revision).

Study participants

We retrospectively collected data from uremic patients undergoing regular hemodialysis or peritoneal dialysis at Nephrology Center of Affiliated Hospital of Jinggangshan University between June 2023 and June 2025 (**Figure 1**). The LDCT protocol used in this study complies with the International Commission on Radiological Protection (ICRP) definition of low-dose CT. We randomly selected dose reports from 30 patients. The results showed that the CT dose index (CTDIvol) ranged from 2.5 to 5.0 mGy, the dose-length product (DLP) ranged from 150 to 350 mGy·cm, and the effective radiation dose was approximately 2.0 to 4.0 mSv. These values are significantly lower than those of conventional diagnostic CT (approxi-

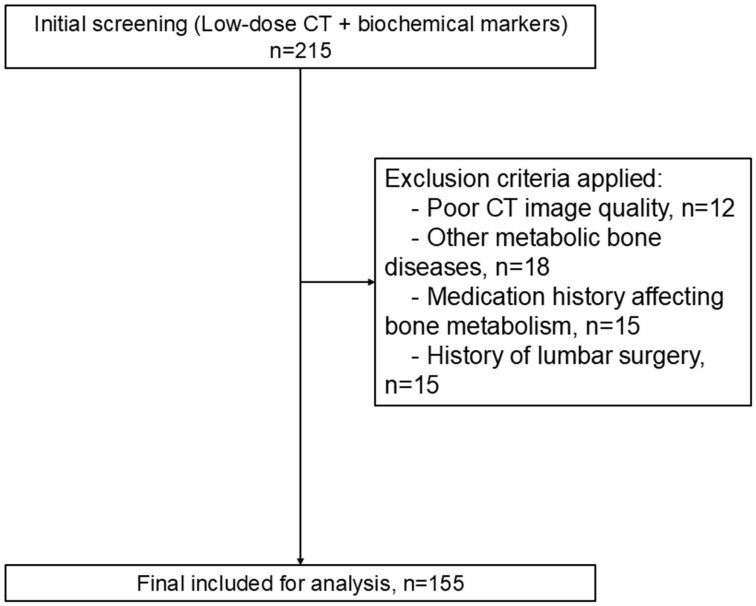

Figure 1. Patient screening flowchart.

mately 5-10 mSv), indicating good radiation safety.

Inclusion and exclusion criteria

Inclusion criteria were as follows: (1) Age ≥18 years; (2) Regular dialysis duration ≥3 months; (3) Completion of an abdominal or pelvic non-contrast low-dose CT scan encompassing the lumbar spine for clinical indications (e.g., assessment of coronary artery calcification, urolithiasis) during the study period; (4) Availability of comprehensive bone metabolic biochemical tests - including intact parathyroid hormone (iPTH), serum calcium, serum phosphorus, alkaline phosphatase (ALP), and 25-hydroxyvitamin D-within 1 month before or after the CT examination.

Exclusion criteria were as follows: (1) History of lumbar spine surgery, fractures, or bone metastases that could affect vertebral structure; (2) Presence of other diseases severely affecting bone metabolism, such as primary hyperparathyroidism, hyperthyroidism, or Paget's disease; (3) Severe CT artifacts precluding accurate measurement; (4) Incomplete clinical or imaging records.

Data collection

The following data were retrospectively collected through the hospital's Electronic Medical Record (EMR) and Picture Archiving and Communication System (PACS).

Demographic and clinical data: Age, sex, dialysis modality, dialysis vintage, Body Mass Index (BMI), and primary renal disease.

Biochemical markers: The most recent results of iPTH, serum calcium, serum phosphorus, ALP, and 25(OH)D closest to the CT examination date were collected. All assays were performed in Affiliated Hospital of Jinggangshan University's clinical laboratory using standardized methods.

CT image data: Original thin-slice images (slice thickness ≤1.25 mm) of low-dose CT scans were retrieved from PACS. CT scanners used included Siemens Somatom Definition Flash, GE Revolution CT, with scanning parameters adhering to a low-dose protocol (tube voltage 100-120 kVp, automated tube current modulation). Scan parameters: Use a Siemens Somatom Definition Flash or GE Revolution CT scanner. The scan field of view covers the abdomen or pelvis. The specific parameters for the low-dose scan protocol are as follows: tube voltage 100-120 kVp; use automatic tube current modulation technology (CARE Dose4D or AutomA) with a reference tube current of 80-120 mAs; pitch 0.8-1.2; Scan speed: 0.5-0.8 seconds per rotation; Reconstruction slice thickness and slice spacing: 0.625-1.25 mm; Reconstruction algorithm: standard soft tissue algorithm or bone algorithm.

Obtain the patient's medication history, including the use of phosphate binders (type and dose), active vitamin D analogs (such as calcitriol and palicalcitol), and calcium-mimetic agents (such as cinacalcet).

CT image analysis and bone microstructural parameter measurement

All CT image analyses were performed independently by two radiologists with more than 3 years of experience in musculoskeletal imaging, who were blinded to the patients' clinical

groupings. The open-source software 3D Slicer (Version 5.2.2) was used for analysis.

Region of Interest (ROI) selection: On axial images, the vertebral body of the first (L1) or second (L2) lumbar vertebra was selected. The superior and inferior endplates, cortical bone, and basivertebral veins were carefully avoided. If L1/L2 were unsuitable due to lesions, the third lumbar vertebra (L3) was selected. In the axial view of the 3D Slicer software, the midsagittal plane of the L1 or L2 vertebral body was selected (avoiding the areas where the vertebral basilar veins enter and exit). The ROI was elliptical, with an area of 200-300 mm^2. The positioning criteria were as follows: the upper border of the ROI was ≥3 mm from the superior endplate; the lower border was ≥3 mm from the inferior endplate; the anterior border was ≥2 mm from the anterior cortical margin of the vertebral body; and the posterior border avoided the area of the vertebral basilar foramen to ensure that the ROI consists primarily of cancellous bone.

Parameter measurements: "Radiomics" or "Quantitative Radiology" module in 3D Slicer version 5.2.2 was used. First, the "Grow from seeds" tool was used or the manual threshold segmentation tool was set to a HU threshold range (e.g., 150-1000 HU) to perform an initial segmentation of the bone tissue. The threshold range was determined based on established methodologies for trabecular bone analysis in CT imaging [18], as threshold selection significantly influences the quantification of bone microstructural parameters [19]. The 'Trabecular Bone Analysis' extension module was applied to automatically calculate microstructural parameters on the segmented binary image using skeletonization and distance transformation algorithms. To calculate BV/TV, the volume of the segmented bone tissue was divided by the total ROI volume; to calculate Tb.Th, Tb.Sp, and Tb.N, measurements based on the plate model were used. An oval-shaped ROI (approximately 200-300 mm^2) was manually delineated within the trabecular bone area, and the software automatically calculated the following quantitative parameters: Volumetric Bone Mineral Density (vBMD): Mean CT value expressed in Hounsfield Units (HU).

Bone Volume Fraction (BV/TV): Percentage of trabecular bone volume relative to total volume.

Trabecular Thickness (Tb.Th): Mean thickness of trabeculae (mm).

Trabecular Separation (Tb.Sp): Mean distance between trabeculae (mm).

Trabecular Number (Tb.N): Number of trabeculae per unit length (1/mm).

Cortical Thickness (Ct.Th): Mean thickness of the lateral vertebral cortex (mm).

The inter-observer ICC values for all six microstructure parameters ranged from 0.846 to 0.884 (Supplementary Table 1), indicating excellent reproducibility. To assess intra-observer reliability, one of the observers randomly selected images from 30 patients and repeated the measurements after a 4-week interval. Intraclass correlation coefficients (ICC) were used to evaluate intra-observer reliability. The results showed that the intra-observer ICC for all parameters was greater than 0.80, indicating excellent reproducibility of the measurements.

Diagnosis and subclassification of ROD

Referencing kidney disease: Improving Global Outcomes (KDIGO) Clinical Practice Guidelines and related literature, patients were diagnosed and subclassified into ROD categories based on biochemical markers (clinical diagnostic criteria, not the gold standard of bone biopsy) as follows.

Non-ROD group: Patients with iPTH, serum calcium, serum phosphorus, and ALP levels all within the target ranges recommended by KDIGO (iPTH: 2-9 times the upper limit of normal; calcium and phosphorus close to normal ranges), without definite clinical evidence of bone disease.

High-turnover ROD: Characterized by significantly elevated iPTH (>600 pg/mL or meeting local laboratory high range), frequently accompanied by hyperphosphatemia and elevated ALP.

Low-turnover ROD: Characterized by low or low-normal iPTH levels (<150 pg/mL), frequently accompanied by hypercalcemia and low ALP.

Mixed-type ROD: Exhibiting biochemical features of both high- and low-turnover disorders, or presenting with intermediate iPTH levels

Table 1. Baseline characteristics

Variable	Overall (N = 155)	Non-ROD (N = 49)	High-turnover ROD (N = 44)	Low-turnover ROD (N = 30)	Mixed-type ROD (N = 32)	F/X^2	*P*-value
Age (years)	54.0 ± 14.4	55.2 ± 14.2	55.2 ± 13.9	50.4 ± 16.1	53.8 ± 13.6	0.844	0.472
Gender - Male (%)	95 (61.3%)	34 (69.4%)	24 (54.5%)	18 (60.0%)	19 (59.4%)	2.268	0.519
Dialysis vintage (years)	7.3 ± 4.2	7.4 ± 4.4	7.7 ± 4.1	7.0 ± 4.2	7.0 ± 4.1	0.246	0.864
BMI (kg/m^2)	24.2 ± 5.1	24.2 ± 4.6	23.9 ± 5.3	24.7 ± 5.6	24.1 ± 5.5	0.133	0.940
Phosphate binder use (%)	87 (56.1%)	14 (28.6%)	34 (77.3%)	13 (43.3%)	26 (81.2%)	33.296	<0.001
Active vitamin D analog use (%)	72 (46.5%)	7 (14.3%)	41 (93.2%)	4 (13.3%)	20 (62.5%)	75.551	<0.001
Calcimimetic use (%)	51 (32.9%)	2 (4.1%)	34 (77.3%)	5 (16.7%)	10 (31.2%)	61.295	<0.001

Abbreviations: ROD, Renal Osteodystrophy; BMI, Body Mass Index; SD, standard deviation.

combined with other marker abnormalities. Final categorization was determined by consensus between two attending nephrologists based on comprehensive biochemical profiles and clinical course.

Statistical analysis

Data analysis was performed using SPSS 26.0 and R 4.2.1 software. Continuous variables that followed a normal distribution are expressed as mean ± standard deviation (Mean ± SD); continuous variables that did not follow a normal distribution are expressed as median (interquartile range); and categorical variables are expressed as frequency (percentage). For between-group comparisons, one-way analysis of variance (ANOVA) was used for data that were normally distributed and had homogeneity of variances; otherwise, the Kruskal-Wallis H test was used. Post-hoc pairwise comparisons were performed using the LSD-t test or Bonferroni correction. Comparisons of categorical variables were performed using the chi-square test or Fisher's exact test. For correlation analysis, Pearson or Spearman correlation is selected based on the data distribution type. Diagnostic performance is evaluated using receiver operating characteristic (ROC) curve analysis, calculating the area under the curve (AUC), optimal cutoff value, sensitivity, and specificity; the DeLong test is used to compare differences in AUC among different models. For multivariate analysis, principal component analysis (PCA) was used to perform dimensionality reduction on multiple CT bone microstructural parameters to explore their primary patterns of variation; if there were differences in baseline medication use among groups, adjustments were made using multivariate analysis of covariance (ANCOVA) or multiple regression analysis. All continuous variables underwent the Shapiro-Wilk normality test prior to correlation analysis. All statistical tests were two-sided, and a *P*-value of <0.05 was considered statistically significant.

Results

Baseline characteristics of the study population

A total of 155 uremic patients undergoing regular dialysis were included in this study, all of whom completed both low-dose CT scans and biochemical assessments of bone metabolism. The mean age of the participants was 54.0 ± 14.4 years, with 61.3% being male. The average dialysis vintage was 7.3 ± 4.2 years. According to the clinical diagnostic criteria, 106 patients (68.4%) were diagnosed with Renal Osteodystrophy (ROD), comprising 44 cases (28.4%) of high-turnover ROD, 30 cases (19.4%) of low-turnover ROD, and 32 cases (20.6%) of mixed-type ROD. The non-ROD group consisted of 49 patients (31.6%). No significant differences were observed among the groups regarding age, sex, dialysis duration, or BMI (**Table 1**). Significant differences were observed among the groups regarding the use of phosphate binders, active vitamin D analogs, and calcimimetics (all *P*<0.001, **Table 1**). Descriptive statistics for biochemical markers and CT-based bone microstructural parameters for the entire cohort are presented in **Table 2**.

Comparison of biochemical markers among ROD subtypes

Significant differences in biochemical markers were observed among the ROD subtypes (**Figure 2**; **Table 3**). Patients with high-turnover ROD exhibited the highest levels of iPTH (552.60 ± 115.90 pg/mL), serum phosphorus

Table 2. Descriptive statistics

Parameter	Mean ± SD	Median	Minimum	Maximum	Reference range	N
iPTH (pg/mL)	251.41 ± 215.77	148.98	11.42	796.07	15-65	155
Serum calcium (mmol/L)	2.31 ± 0.16	2.32	2.00	2.70	2.11-2.52	155
Serum phosphorus (mmol/L)	1.93 ± 0.41	1.91	1.20	2.79	0.85-1.51	155
ALP (U/L)	155.08 ± 80.55	115.39	61.14	340.93	45-125	155
Vitamin D (ng/mL)	21.44 ± 5.47	21.83	10.04	34.29	20-50	155
Volumetric BMD (HU)	157.74 ± 28.05	160.00	80.00	233.00	>150	155
Bone volume fraction (%)	16.49 ± 3.53	16.80	8.00	25.19	15-25	155
Trabecular thickness (mm)	0.13 ± 0.03	0.13	0.08	0.19	0.1-0.2	155
Trabecular separation (mm)	0.89 ± 0.17	0.88	0.48	1.30	0.5-1.0	155
Trabecular number (1/mm)	1.61 ± 0.28	1.60	1.00	2.24	1.5-2.5	155
Cortical thickness (mm)	0.66 ± 0.12	0.67	0.30	0.99	0.5-1.5	155

Abbreviations: iPTH, intact parathyroid hormone; ALP, alkaline phosphatase; BMD, bone mineral density; BV/TV, bone volume fraction; Tb.Th, trabecular thickness; Tb.Sp, trabecular separation; Tb.N, trabecular number; Ct.Th, cortical thickness; HU, Hounsfield Units; SD, standard deviation.

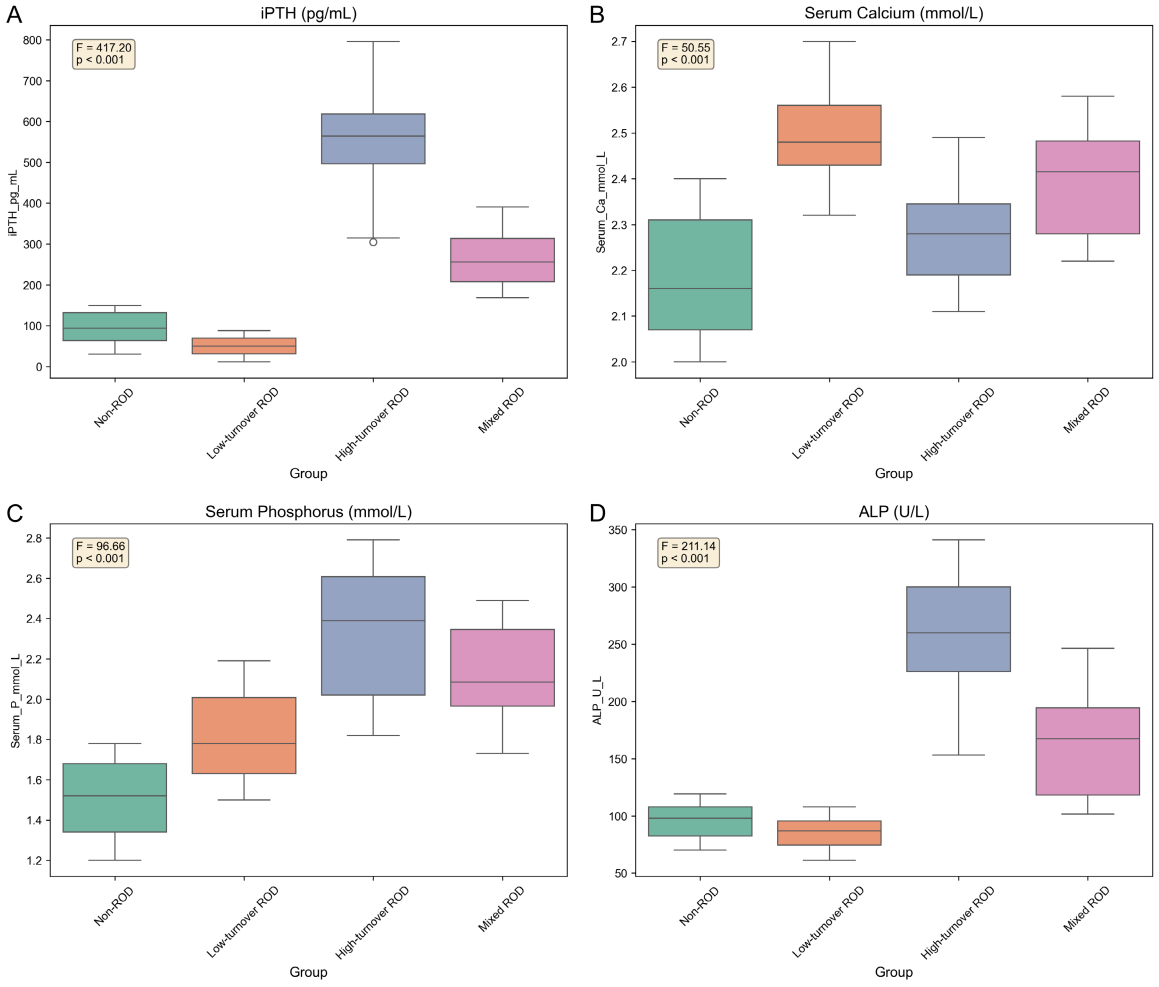

Figure 2. Comparison of biochemical markers among ROD subtypes. Comparison of biochemical markers among ROD subtypes. Box plots showing serum levels of (A) intact parathyroid hormone (iPTH), (B) calcium, (C) phosphorus, (D) alkaline phosphatase (ALP) across the non-ROD (n = 49), high-turnover ROD (n = 44), low-turnover ROD (n = 30), and mixed-type ROD (n = 32) groups. One-way ANOVA revealed significant differences for all markers (P<0.001). Data are presented as mean ± SD. Abbreviations: ROD, Renal Osteodystrophy; iPTH, intact parathyroid hormone; ALP, alkaline phosphatase; SD, standard deviation; ANOVA, analysis of variance.

Table 3. Biochemical ANOVA with descriptive

Variable	Overall (N = 155)	Non-ROD (N = 49)	High-turnover ROD (N = 44)	Low-turnover ROD (N = 30)	Mixed-type ROD (N = 32)	F	*P*-value
iPTH (pg/mL)	251.41 ± 215.77	95.51 ± 35.95	552.60 ± 115.90	50.60 ± 23.29	264.26 ± 61.31	417.203	<0.001
Serum calcium (mmol/L)	2.31 ± 0.16	2.18 ± 0.13	2.28 ± 0.11	2.49 ± 0.10	2.39 ± 0.12	50.553	<0.001
Serum phosphorus (mmol/L)	1.93 ± 0.41	1.51 ± 0.18	2.33 ± 0.32	1.81 ± 0.21	2.13 ± 0.25	96.657	<0.001
ALP (U/L)	155.08 ± 80.55	96.23 ± 15.08	260.55 ± 50.29	85.71 ± 13.39	165.22 ± 46.66	211.14	<0.001

Abbreviations: ROD, Renal Osteodystrophy; iPTH, intact parathyroid hormone; ALP, alkaline phosphatase; SD, standard deviation; ANOVA, analysis of variance.

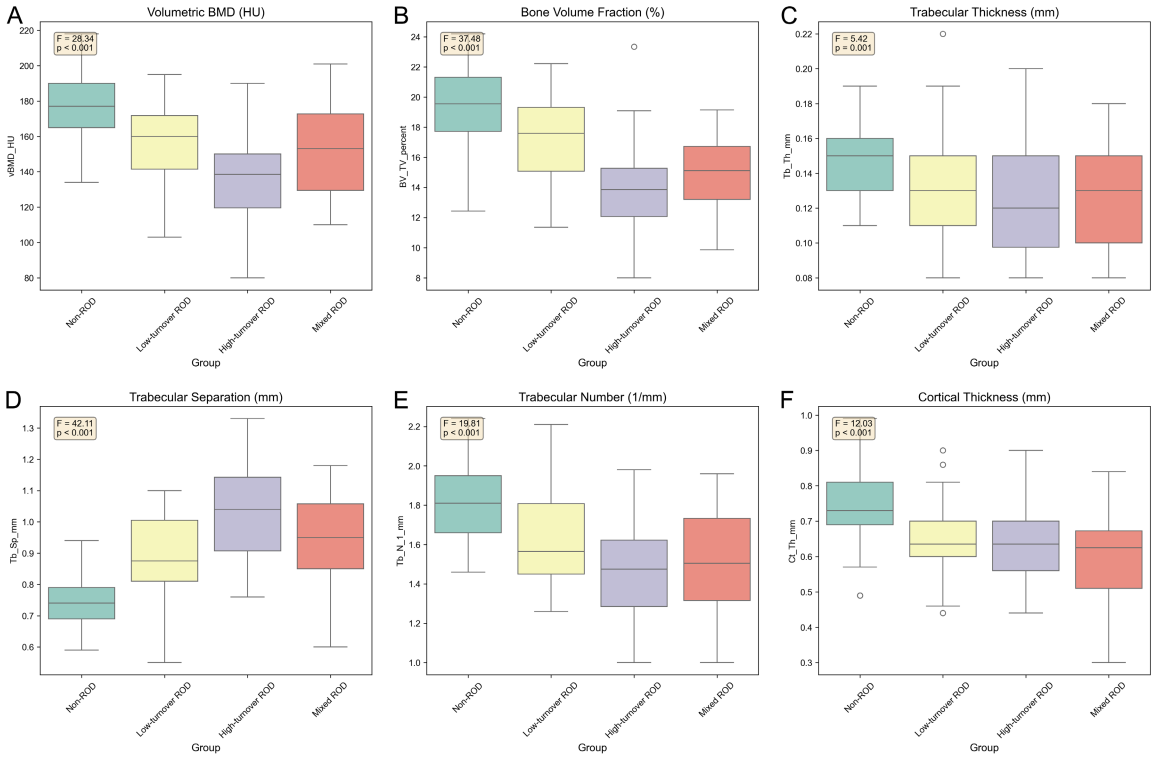

Figure 3. Comparison of CT bone microstructure parameters among ROD subtypes. Comparison of CT-derived bone microstructural parameters among ROD subtypes. Bar charts showing (A) volumetric bone mineral density (vBMD), (B) bone volume fraction (BV/TV), (C) trabecular thickness (Tb.Th), (D) trabecular separation (Tb.Sp), (E) trabecular number (Tb.N), and (F) cortical thickness (Ct.Th) across the non-ROD (n = 49), high-turnover ROD (n = 44), low-turnover ROD (n = 30), and mixed-type ROD (n = 32) groups. One-way ANOVA confirmed significant differences for all parameters (P<0.001, except for Tb.Th: P = 0.001). Data are presented as mean ± SD. Abbreviations: ROD, Renal Osteodystrophy; vBMD, volumetric bone mineral density; BV/TV, bone volume fraction; Tb.Th, trabecular thickness; Tb.Sp, trabecular separation; Tb.N, trabecular number; Ct.Th, cortical thickness; SD, standard deviation; ANOVA, analysis of variance.

(2.33 ± 0.32 mmol/L), and ALP (260.55 ± 50.29 U/L), while showing the lowest vitamin D levels (17.56 ± 4.15 ng/mL). In contrast, patients with low-turnover ROD presented with low iPTH (50.60 ± 23.29 pg/mL), high serum calcium (2.49 ± 0.10 mmol/L), and higher vitamin D levels (27.11 ± 4.51 ng/mL). The mixed-type ROD group displayed values intermediate between these two extremes. One-way ANOVA confirmed that all five biochemical markers differed significantly among the groups (*P*<0.001).

Comparison of CT bone microstructural parameters

CT-derived bone microstructural parameters also showed significant variations across ROD subtypes (**Figure 3**; **Table 4**). Compared to the non-ROD group, all ROD subgroups exhibited lower bone volume fraction (BV/TV), trabecular number (Tb.N), cortical thickness (Ct.Th), and volumetric bone mineral density (vBMD), along with increased trabecular separation (Tb.Sp).

Table 4. CT ANOVA with Descriptive

Variable	Overall (N = 155)	Non-ROD (N = 49)	High-turnover ROD (N = 44)	Low-turnover ROD (N = 30)	Mixed-type ROD (N = 32)	F	*P*-value
Volumetric BMD (HU)	157.74 ± 28.05	178.86 ± 18.74	135.77 ± 22.66	159.53 ± 21.78	153.91 ± 28.31	28.340	<0.001
Bone volume fraction (%)	16.49 ± 3.53	19.43 ± 2.56	13.89 ± 3.09	17.22 ± 2.72	14.88 ± 2.30	37.480	<0.001
Trabecular thickness (mm)	0.13 ± 0.03	0.15 ± 0.02	0.13 ± 0.03	0.13 ± 0.03	0.13 ± 0.03	5.422	<0.001
Trabecular separation (mm)	0.89 ± 0.17	0.74 ± 0.08	1.03 ± 0.15	0.89 ± 0.14	0.94 ± 0.14	42.109	<0.001
Trabecular number (1/mm)	1.61 ± 0.28	1.81 ± 0.20	1.45 ± 0.24	1.64 ± 0.25	1.51 ± 0.27	19.814	<0.001
Cortical thickness (mm)	0.66 ± 0.12	0.73 ± 0.10	0.63 ± 0.10	0.65 ± 0.10	0.60 ± 0.13	12.034	<0.001

Abbreviations: ROD, Renal Osteodystrophy; BMD, bone mineral density; BV/TV, bone volume fraction; Tb.Th, trabecular thickness; Tb.Sp, trabecular separation; Tb.N, trabecular number; Ct.Th, cortical thickness; HU, Hounsfield Units; SD, standard deviation; ANOVA, analysis of variance.

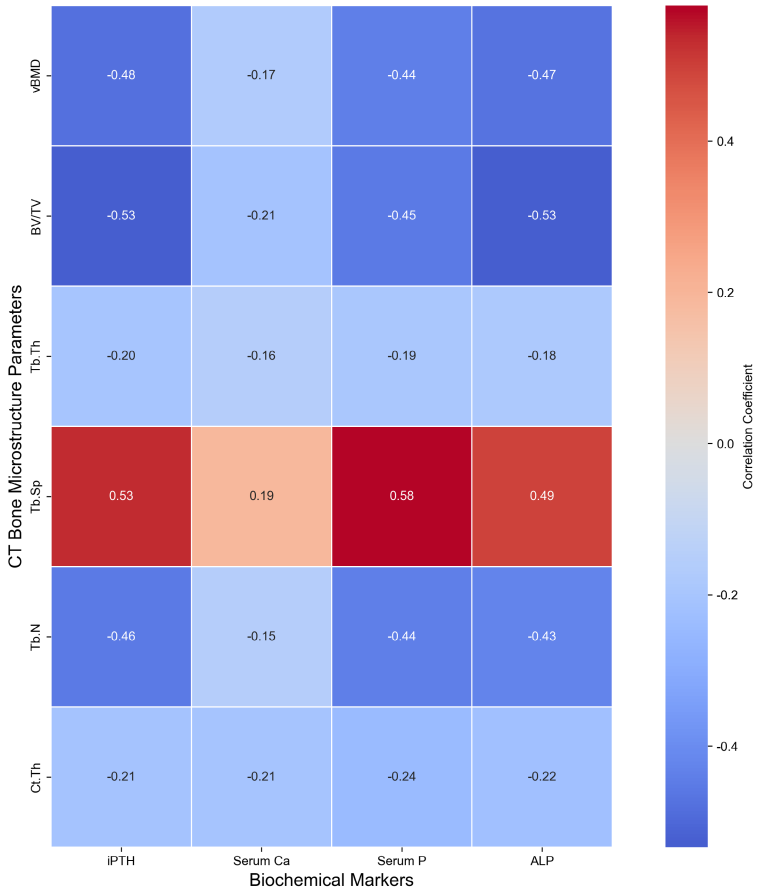

Figure 4. Correlation between CT parameters and biochemical markers. Abbreviations: CT, computed tomography; iPTH, intact parathyroid hormone; ALP, alkaline phosphatase; vBMD, volumetric bone mineral density; BV/TV, bone volume fraction; Tb.Th, trabecular thickness; Tb.Sp, trabecular separation; Tb.N, trabecular number; Ct.Th, cortical thickness.

Notably, the high-turnover ROD subtype demonstrated the most severe microstructural deterioration, characterized by the lowest BV/TV (13.89 ± 3.09%) and vBMD (135.77 ± 22.66 HU), as well as the highest Tb.Sp (1.03 ± 0.15 mm). One-way ANOVA confirmed highly significant differences for all CT parameters among the groups (*P*<0.001).

Correlation between CT parameters and biochemical markers

Correlation analysis (**Figure 4**) revealed significant associations between biochemical markers reflecting bone resorption and metabolic activity (iPTH, phosphorus, ALP) and CT bone microstructural parameters. Specifically, BV/TV, vBMD, and Tb.N showed moderate to strong negative correlations with iPTH, phosphorus, and ALP (correlation coefficients r ranging from -0.429 to -0.534, *P*<0.001). Conversely, Tb.Sp showed positive correlations with these markers (correlation coefficients *r* ranging from 0.494 to 0.579, P<0.001). The correlations between serum calcium and CT parameters were relatively weak. Since the iPTH and dialysis duration followed a non-normal distribution (Shapiro-Wilk test, P<0.05), Spearman's correlation analysis was used to assess their correlation with CT parameters; Pearson's correlation analysis was used for the remaining variables.

Association of bone microstructure with vascular calcification and fracture risk

To further explore the relationship between bone microstructure changes and the multisystem transformation effects of metabolic bone diseases, this study analyzed the correlations between CT bone microstructure param-

Table 5. Correlations between bone microstructure parameters and vascular calcification, fracture risk

Microstructure parameter	Outcome	Correlation coefficient (r)	*P*-value	Method
Bone volume fraction (%)	Coronary artery calcification (CAC)	-0.383	<0.001	Spearman
Bone volume fraction (%)	Fragility fracture history	-0.047	0.557	Spearman
Trabecular separation (mm)	Coronary artery calcification (CAC)	0.131	0.104	Spearman
Trabecular separation (mm)	Fragility fracture history	0.120	0.138	Spearman
Volumetric BMD (HU)	Coronary artery calcification (CAC)	-0.159	0.048	Spearman
Volumetric BMD (HU)	Fragility fracture history	-0.028	0.729	Spearman
Trabecular number (1/mm)	Coronary artery calcification (CAC)	-0.016	0.845	Spearman
Trabecular number (1/mm)	Fragility fracture history	0.050	0.535	Spearman
Cortical thickness (mm)	Coronary artery calcification (CAC)	-0.160	0.046	Spearman
Cortical thickness (mm)	Fragility fracture history	0.024	0.769	Spearman

Abbreviations: ROD, Renal Osteodystrophy; CAC, coronary artery calcification; BMD, bone mineral density; HU, Hounsfield Units; BV/TV, bone volume fraction; Tb.Sp, trabecular separation; Tb.N, trabecular number; Ct.Th, cortical thickness; SD, standard deviation.

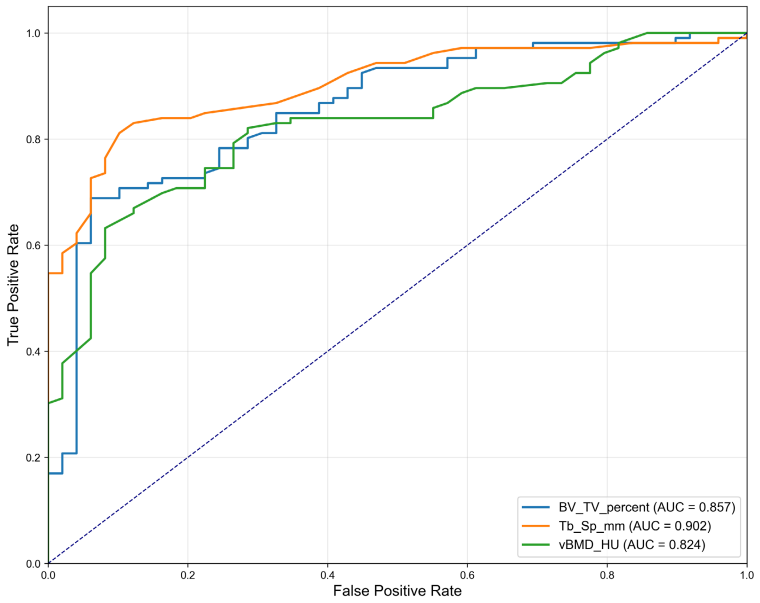

Figure 5. ROC curves of key CT parameters for ROD diagnosis. Abbreviations: ROD, Renal Osteodystrophy; ROC, Receiver Operating Characteristic; AUC, Area Under the Curve; Tb.Sp, trabecular separation; BV/TV, bone volume fraction; vBMD, volumetric bone mineral density.

eters and coronary artery calcium score (CAC) as well as the history of fragility fractures (**Table 5**). The results showed that the bone volume fraction (BV/TV) was significantly negatively correlated with CAC (r = -0.383, P<0.001), indicating that the more severe the bone loss, the higher the degree of vascular calcification. The volumetric bone density (vBMD) and cortical bone thickness (Ct.Th) were also weakly but statistically significantly negatively correlated with CAC (r = -0.159 and -0.160 respectively, both P< 0.05). The trabecular separation (Tb.Sp) was positively correlated with CAC, but did not reach statistical significance (r = 0.131, P = 0.104). In terms of fracture risk, all bone microstructure parameters were not significantly correlated with the history of fragility fractures (all P>0.05).

Diagnostic performance of CT parameters for ROD

Receiver Operating Characteristic (ROC) curve analysis was used to evaluate the diagnostic value of key CT parameters in differentiating ROD from non-ROD (**Figure 5**). Trabecular separation (Tb.Sp) demonstrated the highest diagnostic performance, with an Area Under the Curve (AUC) of 0.902. At an optimal cutoff value of 0.84 mm, it yielded a sensitivity of 81.1% and a specificity of 89.8%. The AUCs for bone volume fraction (BV/TV) and volumetric bone mineral density (vBMD) were 0.857 and 0.824, respectively. When a combined model was constructed by integrating standardized iPTH and BV/TV parameters, the diagnostic AUC improved to 0.888, outperforming either individual indicator alone (**Figure 6**).

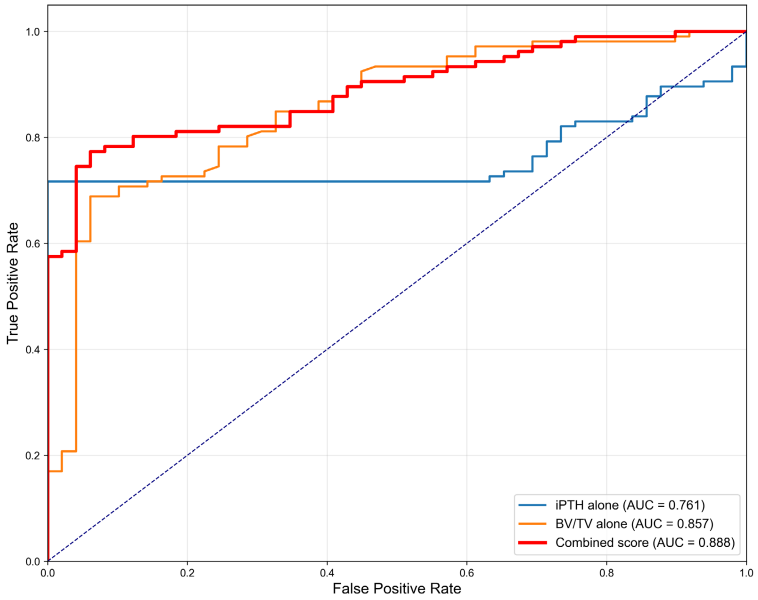

Figure 6. ROC curves of combined diagnostic model. Abbreviations: ROD, Renal Osteodystrophy; ROC, Receiver Operating Characteristic; AUC, Area Under the Curve; iPTH, intact parathyroid hormone; BV/TV, bone volume fraction.

Comparison of parameter differences among ROD subtypes

Forest plots visually illustrate the mean differences in key indicators between each ROD subtype and the non-ROD group (**Figure 7**). The results showed that high-turnover and mixed-type ROD exhibited significant positive or negative differences compared to the non-ROD group in terms of iPTH, serum phosphorus, ALP, and most CT parameters. In contrast, low-turnover ROD was primarily characterized by significantly lower iPTH and ALP levels, and higher serum calcium levels compared to the non-ROD group. Representative mean comparisons of key parameters across subtypes are shown in **Figure 8**.

Association between dialysis vintage and bone microstructure

A significant negative correlation was observed between dialysis vintage and bone volume fraction (BV/TV) (r = -0.261, P = 0.001), suggesting that bone loss may intensify as the duration of dialysis increases (**Figure 9**). The linear regression equation was: BV/TV (%) = 18.11 - 0.22 × Dialysis vintage (years).

Principal component analysis of bone microstructural parameters

Principal Component Analysis (PCA) was performed on the six CT bone microstructural parameters for dimensionality reduction (**Figure 10**). The first two principal components accounted for 56.0% of the total variance (PC1: 40.5%, PC2: 15.4%), indicating that these parameters can effectively distinguish different bone microstructural phenotypes and may correspond to distinct ROD pathophysiological states.

Discussion

This study systematically investigated the value of quantitative assessment of lumbar vertebral microstructure using routine low-dose CT (LDCT) images for the non-invasive diagnosis of Renal Osteodystrophy (ROD) through a retrospective analysis of 155 uremic patients undergoing regular dialysis. The main findings were as follows: (1) Distinctive alterations in CT-based bone microstructural parameters were observed among different ROD subtypes, which corresponded to the classical patterns of biochemical abnormalities; (2) Parameters such as trabecular separation (Tb.Sp) demonstrated excellent diagnostic performance for identifying ROD; (3) CT microstructural parameters showed significant correlations with key biochemical markers (iPTH, ALP, serum phosphorus) reflecting bone metabolic activity; (4) A combined model integrating iPTH and bone volume fraction (BV/TV) further enhanced diagnostic accuracy. These results provide important imaging evidence for utilizing the widely available LDCT as a tool for the auxiliary diagnosis and evaluation of ROD.

The most significant finding of this study is that bone microstructural parameters derived from routine LDCT can effectively differentiate between various ROD subtypes. Our data revealed that patients with high-turnover ROD exhibited the most severe microstructural deterioration, characterized by the greatest Tb.Sp and the

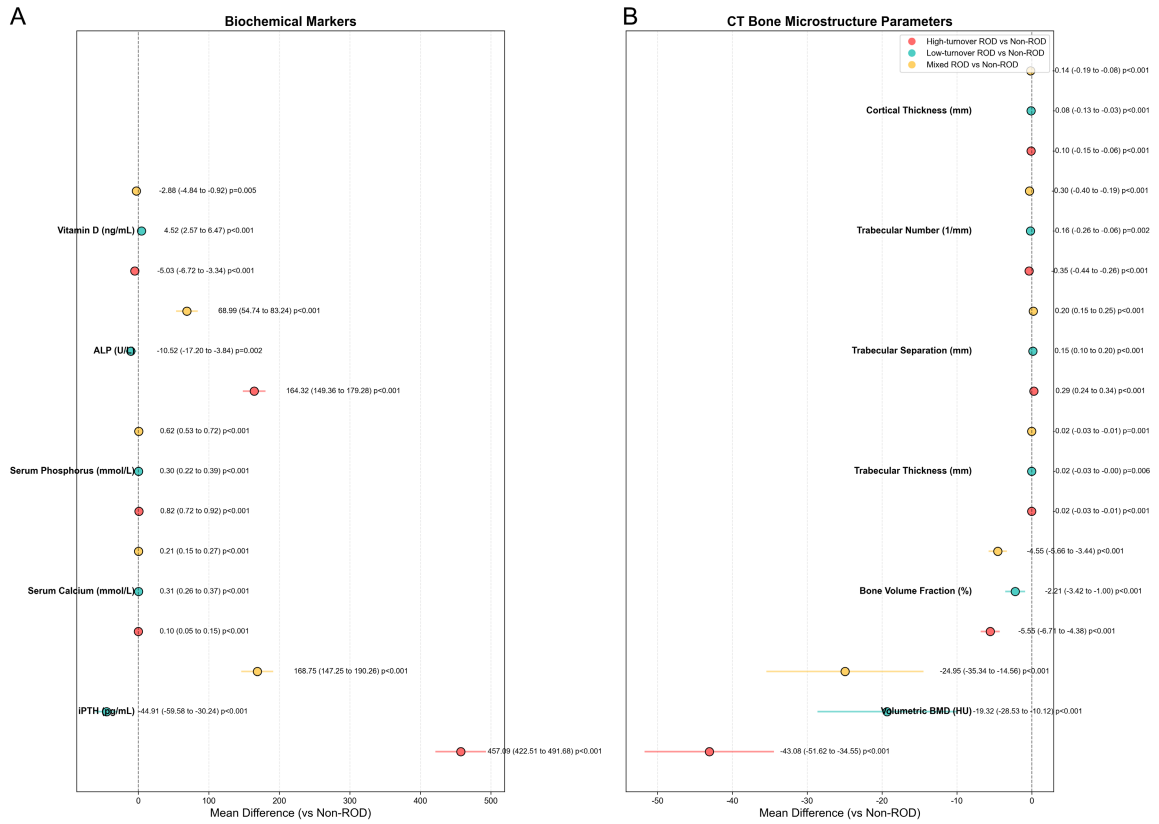

Figure 7. Forest plot of mean differences between ROD subtypes and non-ROD group. Forest plot of mean differences between each ROD subtype and the non-ROD group. A. Biochemical markers: iPTH, serum calcium, serum phosphorus, ALP, and vitamin D. B. CT bone microstructural parameters: vBMD, BV/TV, Tb.Th, Tb.Sp, Tb.N, and Ct.Th. Mean differences with 95% confidence intervals are shown. A positive mean difference indicates higher values in the ROD subtype compared with the non-ROD group, whereas a negative mean difference indicates lower values. *P*-values were derived from post-hoc pairwise comparisons following one-way ANOVA. Abbreviations: ROD, Renal Osteodystrophy; iPTH, intact parathyroid hormone; ALP, alkaline phosphatase; vBMD, volumetric bone mineral density; BV/TV, bone volume fraction; Tb.Th, trabecular thickness; Tb.Sp, trabecular separation; Tb.N, trabecular number; Ct.Th, cortical thickness; SD, standard deviation; CI, confidence intervals; ANOVA, analysis of variance.

lowest BV/TV, trabecular number (Tb.N), and volumetric bone mineral density (vBMD). This observation is highly consistent with the underlying pathophysiology: persistent high levels of PTH stimulate excessive osteoclastic activity, leading to accelerated bone resorption, thinning and fracturing of trabeculae, increased inter-trabecular spacing, and severe bone loss [20, 21]. Notably, patients with low-turnover ROD showed relatively milder microstructural impairment, with lower Tb.Sp and higher BV/TV and vBMD compared to the high-turnover group. This may reflect a state of suppressed bone remodeling where both resorption and formation are low, resulting in a relatively "quiescent" bone structure that has not undergone the severe destructive process characteristic of high-turnover disease [22, 23]. The parameters for mixed-type ROD fell between these two extremes, reflecting the complexity of its pathological changes. These findings confirm that quantitative CT microstructural analysis can non-invasively reflect the distinct histological patterns underlying different ROD subtypes, serving as a powerful complement to traditional biochemical classification.

In our study, Tb.Sp exhibited the highest discriminative ability for diagnosing ROD (AUC = 0.902). Tb.Sp intuitively reflects the sparseness of the trabecular network and is a key microstructural determinant of decreased bone strength and increased fracture risk [24]. Its superior diagnostic performance suggests that the "qualitative change" in bone structure (e.g., loss of trabecular connectivity) may be as

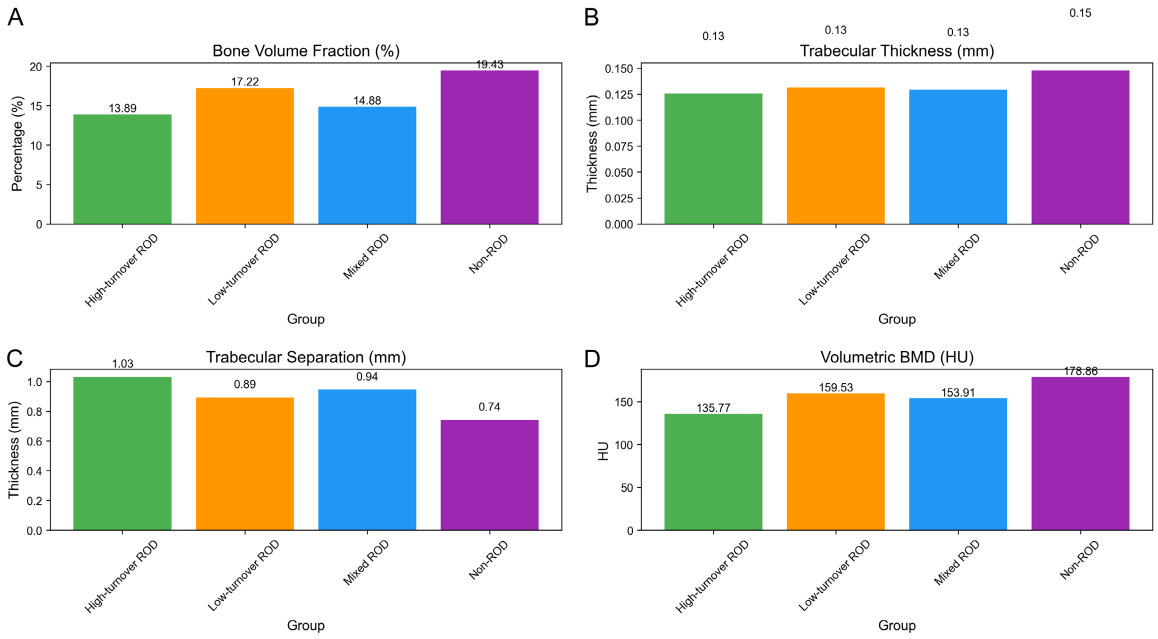

Figure 8. Mean values of key parameters by ROD subtype. Mean values of key parameters by ROD subtype. Bar charts showing the mean values of (A) bone volume fraction (BV/TV), (B) trabecular thickness (Tb.Th), (C) trabecular separation (Tb.Sp), and (D) volumetric bone mineral density (vBMD) in the non-ROD, high-turnover ROD, low-turnover ROD, and mixed-type ROD groups. Data are presented as mean values. Significant inter-group differences were observed for all parameters (see **Figure 3** and **Table 4** for detailed statistics). Abbreviations: ROD, Renal Osteodystrophy; BV/TV, bone volume fraction; Tb.Th, trabecular thickness; Tb.Sp, trabecular separation; vBMD, volumetric bone mineral density; SD, standard deviation.

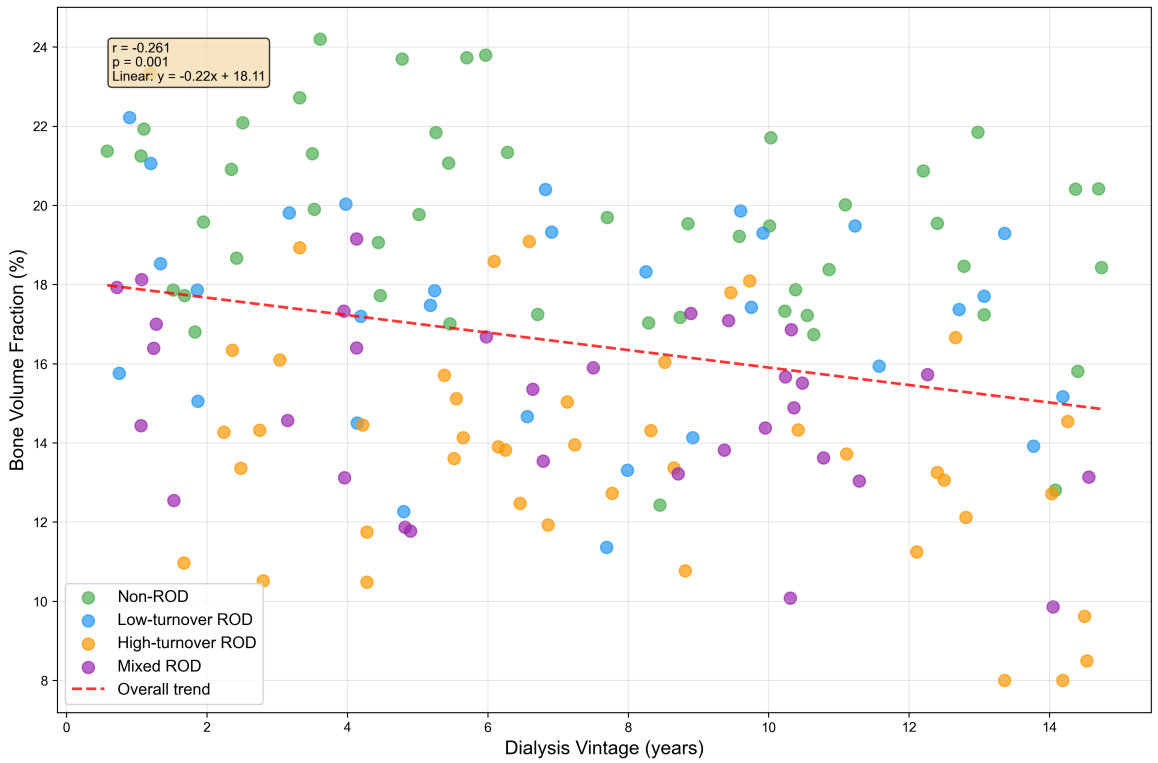

Figure 9. Relationship between dialysis vintage and bone volume fraction. Abbreviation: BV/TV, bone volume fraction.

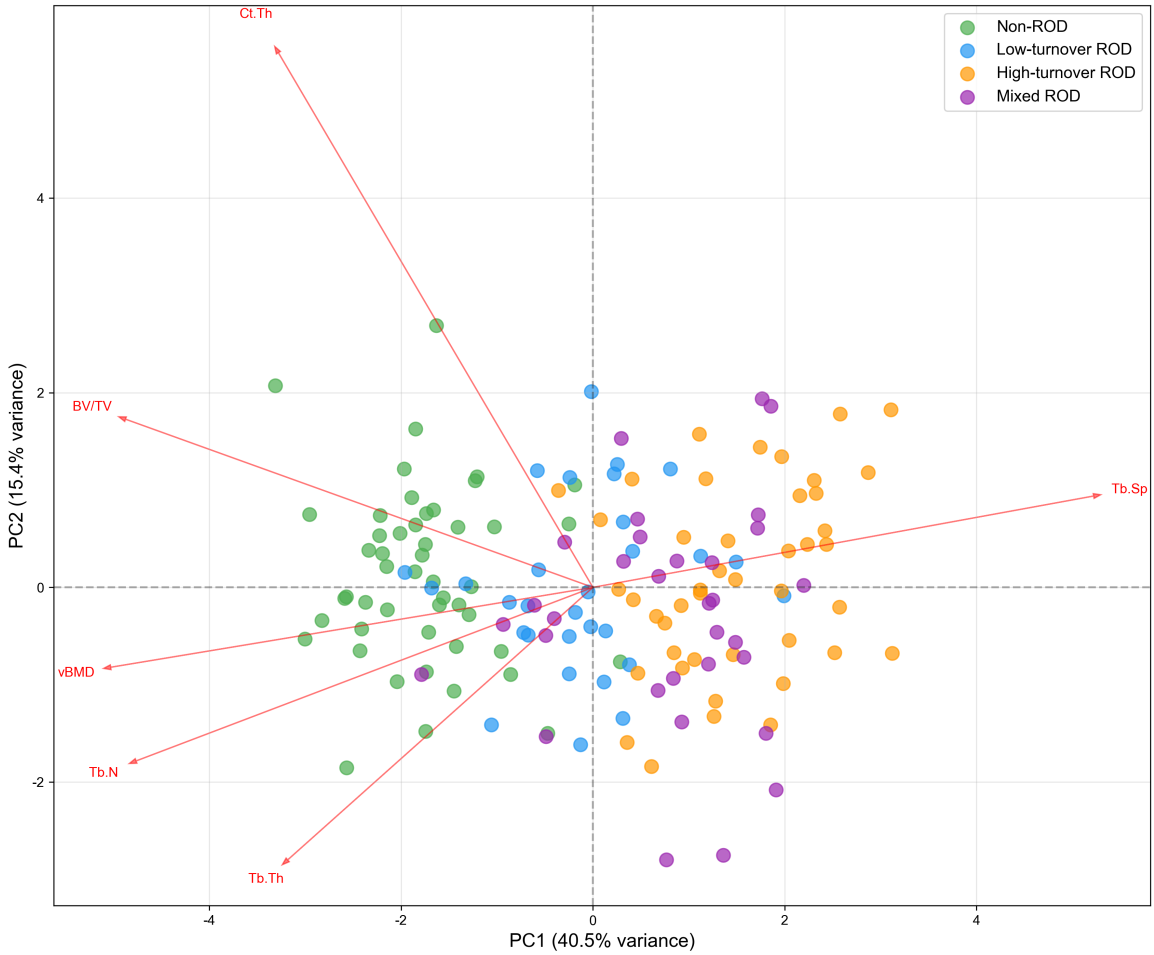

Figure 10. PCA of bone microstructure parameters. Abbreviations: CT, computed tomography; PCA, Principal Component Analysis.

important as, or even more critical than, the "quantitative change" (e.g., decline in bone density) when evaluating bone disease in uremic patients. This finding is consistent with studies using high-resolution peripheral quantitative CT (HR-pQCT) in ROD patients, which have also confirmed that trabecular structural parameters are important indicators for distinguishing bone turnover states [25-27]. The innovation of our study lies in successfully applying this concept to the more widely available routine LDCT and establishing a specific diagnostic threshold (0.84 mm) through ROC analysis, thereby providing a concrete reference for clinical translation. Furthermore, BV/TV and vBMD also demonstrated good diagnostic value, further supporting the necessity of a comprehensive assessment combining both bone quantity and quality.

Correlation analysis revealed biologically plausible links between CT parameters and biochemical markers. iPTH, ALP, and serum phosphorus showed positive correlations with Tb.Sp and negative correlations with BV/TV and vBMD. This association reinforces a central concept: biochemical markers reflecting high bone turnover are closely linked to imaging manifestations of deteriorating bone architecture. This provides a rationale for using readily available biochemical tests to preliminarily gauge the extent of underlying structural bone damage in clinical practice [28, 29]. However, it is important to note that these correlations were only moderate, indicating that biochemical markers cannot fully substitute for direct assessment of bone structure. Discrepancies between biochemical profiles and histological/radiological findings may exist in some patients;

in such cases, CT quantitative analysis may offer more direct and accurate information [30, 31].

Compared with traditional dual-energy X-ray absorptiometry (DXA), LDCT not only assesses bone mineral density (vBMD) but also provides key information on bone microstructure (e.g., Tb.Sp), whereas DXA cannot distinguish between microstructural changes in trabecular and cortical bone. Compared to high-resolution peripheral quantitative computed tomography (HR-pQCT), although HR-pQCT offers superior capabilities in assessing peripheral bone microstructure, it suffers from low equipment availability and limited scanning sites. The LDCT used in this study is a widely adopted imaging modality in the follow-up of patients with uremia. It provides "one-stop" information on lumbar spine bone microstructure without requiring additional radiation exposure or costs, offering unique advantages in terms of clinical accessibility and cost-effectiveness.

The diagnostic model combining iPTH and BV/TV demonstrated an AUC (0.888) superior to either individual parameter. This highlights the advantage of multimodal data integration: iPTH provides a systemic biochemical signal of bone metabolic activity, whereas BV/TV offers structural information on vertebral bone mass. Together, they capture both functional abnormalities and structural consequences, theoretically enhancing the comprehensiveness and robustness of the diagnosis. This suggests that future development of automated diagnostic tools should consider fusing clinical and imaging data.

The findings of this study carry significant clinical utility. For long-term dialysis patients, routine LDCT scans - already performed for assessing vascular calcification or other complications - can be "repurposed" to simultaneously evaluate lumbar vertebral status. This approach requires no additional scanning, incurs no incremental radiation burden, is non-invasive, and highly cost-effective. It holds promise as a screening or adjunctive diagnostic tool in clinical practice, aiding in the identification of high-risk patients with severe microstructural deterioration, thereby guiding more aggressive interventions (e.g., adjustment of phosphate binders, active vitamin D, or calcimimetics) and potentially monitoring treatment response.

It is worth noting that this study found that the bone volume fraction (BV/TV) was significantly negatively correlated with coronary artery calcification (CAC), which is consistent with the emerging research concept of the bone-vascular axis in chronic kidney disease (CKD). This result suggests that common pathological driving factors such as chronic inflammation, oxidative stress, and imbalance of the RANKL/RANK/OPG pathway may simultaneously promote bone resorption and vascular calcification. Although this study was of a cross-sectional design and could not infer causality, the data preliminarily confirm that low-dose spiral CT (LDCT) can simultaneously assess bone fragility and cardiovascular risk, and has unique advantages compared to traditional bone density testing.

This study does have several limitations. First, as a single-center retrospective analysis, it inevitably involves selection bias and has a limited sample size; therefore, its external validity requires further validation through multicenter prospective studies. Second, the most significant limitation lies in the fact that the diagnosis and subtyping of renal osteodystrophy (ROD) were based on clinical and biochemical indicators rather than bone biopsy, the gold standard. This may lead to a certain degree of misclassification and selection bias [32, 33]. However, addressing this gap - namely, identifying the optimal non-invasive alternative when biopsy is not feasible - is precisely the clinical challenge this study aims to resolve. Third, the CT measurements in this study were based on two-dimensional region-of-interest (ROI) analysis rather than true three-dimensional morphological assessment, which may have limited measurement precision to some extent compared with high-resolution peripheral quantitative computed tomography (HR-pQCT) [34]. Furthermore, future studies could explore AI-based whole-vertebra segmentation and three-dimensional parameter extraction techniques to further improve analytical efficiency and accuracy. No significant correlation was observed between the CT microscopic structural parameters and the existing fragility fractures. This might be due to the limited sample size of fracture events in this cross-sectional cohort.

Moreover, the fracture risk of uremic patients is influenced by multiple factors such as falls and neuromuscular function impairment. Future prospective studies are still needed to verify the predictive value of these parameters for new fractures.

Conclusion

This study confirms that quantitative analysis of lumbar spine microstructure using low-dose CT (LDCT) images - which are already part of routine examinations for patients with uremia - is a non-invasive assessment tool with promising clinical applications. This method can effectively distinguish between different subtypes of renal osteodystrophy (ROD), with trabecular bone separation (Tb.Sp) demonstrating the highest diagnostic performance. Significant correlations were observed between CT microstructural parameters and key serum biochemical markers (such as iPTH and ALP), and a model combining imaging parameters (BV/TV) with biochemical markers (iPTH) further improved diagnostic accuracy. This study provides empirical evidence for the non-invasive and convenient assessment of ROD using widely accessible LDCT, which aids in the early identification of high-risk patients and guides personalized treatment in clinical practice, while avoiding the limitations of invasive bone biopsy. Based on these findings, we propose the following clinical recommendations: For patients on long-term dialysis, quantitative analysis of lumbar spine microstructure can be performed concurrently with routine LDCT examinations (e.g., for assessing vascular calcification). If Tb.Sp >0.84 mm or BV/TV <16.5%, indicating a high risk of ROD, further stratification should be conducted in conjunction with biochemical markers such as iPTH to guide adjustments to treatment regimens, including active vitamin D or phosphate binders. Future multicenter prospective studies and the development of automated analysis workflows are needed to further validate the reliability of this method and its predictive value for clinical hard endpoints such as fractures, as well as to explore its potential applications in the dynamic monitoring of treatment.

Disclosure of conflict of interest

None.

Address correspondence to: Rencong Xu, Department of Nephrology, Ganzhou People's Hospital, No. 16, Meiguan Avenue, Zhangguang District, Ganzhou 341000, Jiangxi, China. Tel: +86-0797-5889952; E-mail: xrczzz@163.com

References

[1] Hicks RJ, Ware RE and Callahan J. Total-body PET/CT: pros and cons. Semin Nucl Med 2025; 55: 11-20.

[2] Yang Q, Chen S, Yu Z, Wen X and Ou S. Advances in noninvasive diagnosis of renal osteodystrophy. Ren Fail 2025; 47: 2593710.

[3] Barabasová P, Kováčová V, Stejskal P, Unčovský M, Valterová E and Vystavěl T. Tuneable in-situ nanoCT workflow using FIB/SEM. Ultramicroscopy 2021; 225: 113283.

[4] Lai KKH, Aljufairi FMAA, Sebastian JU, Yip CCY, Wei Y, Jia R, Cheuk W, Cheng ACO, Chin JKY, Chu CY, Kwong CH, Yip NKF, Li KKW, Chan WH, Yip WWK, Young AL, Chan E, Ko CKL, Chan CKM, Yuen HKL, Chen LJ, Tham CCY, Pang CP and Chong KKL. Systemic involvement in immunoglobulin G4-related ophthalmic disease. Ocul Immunol Inflamm 2024; 32: 1852-1858.

[5] Cheung YC, Yee DK and Fang C. Defining the fit and ideal entry site of the fibula rod system–a computed tomography based study in elderly patients with lower limb infections, vascular diseases or tumors. J Orthop Surg (Hong Kong) 2023; 31: 10225536231157129.

[6] Haemmerli J, Ferdowssian K, Wessels L, Mertens R, Hecht N, Woitzik J, Schneider UC, Bayerl SH, Vajkoczy P and Czabanka M. Comparison of intraoperative CT- and cone beam CT-based spinal navigation for the treatment of atlantoaxial instability. Spine J 2023; 23: 1799-1807.

[7] Hasegawa A, Ichikawa K, Morioka Y and Kawashima H. A tin filter's dose reduction effect revisited: using the detectability index in low-dose computed tomography for the chest. Phys Med 2022; 99: 61-67.

[8] Putha SK, Lobo D, Raghvendra H, Srinvias C, Banerjee S, Athiyamaan MS, Sunny KJ and Krishna A. Evaluation of inhomogeneity correction performed by radiotherapy treatment planning system. Asian Pac J Cancer Prev 2022; 23: 4155-4162.

[9] Ma T, Wei Q, Lyu Z, Zhang D, Zhang H, Wang R, Dong J, Liu Y, Yao R and He ZX. Self-collimating SPECT with multi-layer interspaced mosaic detectors. IEEE Trans Med Imaging 2021; 40: 2152-2169.

[10] Yoshida E, Akamatsu G, Tashima H, Kamada K, Yoshikawa A and Yamaya T. First imaging dem-

onstration of a crosshair light-sharing PET detector. Phys Med Biol 2021; 66: 065013.
[11] Tomita Y, Ichikawa Y, Hashizume K and Sakuma H. Effect of Gaussian smoothing filter size for CT-based attenuation correction on quantitative assessment of bone SPECT/CT: a phantom study. J Digit Imaging 2023; 36: 2313-2321.
[12] Matsuura K, Ichikawa K and Kawashima H. Task-specific spatial resolution properties of iterative and deep learning-based reconstructions in computed tomography: Comparison using tasks assuming small and large enhanced vessels. Phys Med 2022; 95: 64-72.
[13] Imamura E, Mayahara M, Inoue S, Miyamoto M, Funae T, Watanabe Y, Matsuki-Fukushima M and Nakamura M. Trabecular structure and composition analysis of human autogenous bone donor sites using micro-computed tomography. J Oral Biosci 2021; 63: 74-79.
[14] You T, Meng Y, Wang Y and Chen H. CT diagnosis of the fracture of anterior nasal spine. Ear Nose Throat J 2022; 101: Np45-NP49.
[15] Hiyama A, Katoh H, Sakai D, Sato M and Watanabe M. Minimally invasive approach for degenerative spondylolisthesis: lateral single-position surgery with intraoperative computed tomography navigation and fluoroscopy: a technical note. World Neurosurg 2023; 179: e500-e509.
[16] Vaz SC, Adam JA, Delgado Bolton RC, Vera P, van Elmpt W, Herrmann K, Hicks RJ, Lievens Y, Santos A, Schöder H, Dubray B, Visvikis D, Troost EGC and de Geus-Oei LF. Perspective paper about the joint EANM/SNMMI/ESTRO practice recommendations for the use of 2-[(18)F]FDG-PET/CT external beam radiation treatment planning in lung cancer. Radiother Oncol 2022; 168: 37-39.
[17] Tsuboi K, Kanbe T, Matsushima H, Ohtani Y, Tanikawa K and Kaneko M. Three-dimensional CT imaging in extensor tendons using deep learning reconstruction: optimal reconstruction parameters and the influence of dose. Phys Eng Sci Med 2023; 46: 1659-1666.
[18] Buyuksungur A, Szabó BT, Dobai A and Orhan K. The effect of micro-computed tomography thresholding methods on bone micromorphometric analysis. J Funct Biomater 2024; 15: 343.
[19] Marques ML, da Silva NP, van der Heijde D, Reijnierse M, Baraliakos X, Braun J, van Gaalen F and Ramiro S. Hounsfield Units measured in low dose CT reliably assess vertebral trabecular bone density changes over two years in axial spondyloarthritis. Semin Arthritis Rheum 2023; 58: 152144.
[20] Chen S, Li B, Liu S, Zhao J, Zhou X, Zhai X, Gu X, Hou C, Shi Z, Bai Y, Li M and Mao N. Sagittal imaging study of the lumbar spine with the short rod technique. Eur Spine J 2022; 31: 3536-3543.
[21] Guevar J, Samer ES, Precht C, Rathmann JMK and Forterre F. Accuracy and safety of neuronavigation for minimally invasive stabilization in the thoracolumbar spine using polyaxial screws-rod: a canine cadaveric proof of concept. Vet Comp Orthop Traumatol 2022; 35: 370-380.
[22] Pu X, Wang X, Ran L, Xie T, Li Z, Yang Z, Lin R and Zeng J. Comparison of predictive performance for cage subsidence between CT-based Hounsfield units and MRI-based vertebral bone quality score following oblique lumbar interbody fusion. Eur Radiol 2023; 33: 8637-8644.
[23] Xin L, Luo J, Chen M, He B, Tang B, Tang C, Zhang D and Zhang L. Anatomy and correlation of the coracoid process and coracoclavicular ligament based on three-dimensional computed tomography reconstruction and magnetic resonance imaging. Med Sci Monit 2021; 27: e930435.
[24] Lin CS, Tsai YC, Chen LH, Wang CW, Wu CJ, Chen WY, Liang HK and Kuo SH. Effect of extended field-of-view approaches on the accuracy of stopping power ratio estimation for single-energy computed tomography simulators. J Appl Clin Med Phys 2023; 24: e14010.
[25] Koria L, Farndon M, Jones E, Mengoni M and Brockett C. Changes in subchondral bone morphology with osteoarthritis in the ankle. PLoS One 2024; 19: e0290914.
[26] Porrelli D, Abrami M, Pelizzo P, Formentin C, Ratti C, Turco G, Grassi M, Canton G, Grassi G and Murena L. Trabecular bone porosity and pore size distribution in osteoporotic patients - a low field nuclear magnetic resonance and microcomputed tomography investigation. J Mech Behav Biomed Mater 2022; 125: 104933.
[27] Ren L, Sun Y, Yeh B, Marsh JF, Winfree TN, Burke KA, Rajendran K, McCollough CH, Mileto A, Fletcher JG and Leng S. Characterization of single- and multi-energy CT performance of an oral dark borosilicate contrast media using a clinical photon-counting-detector CT platform. Med Phys 2023; 50: 6779-6788.
[28] Xu L, Hu YJ, Peng Y, Wang Z, Wang J, Lu WW, Tang B and Guo XE. Early zoledronate treatment inhibits subchondral bone microstructural changes in skeletally-mature, ACL-transected canine knees. Bone 2023; 167: 116638.
[29] Prieto E, Irazola L, Collantes M, Ecay M, Cuenca T, Martí-Climent JM and Peñuelas I. Performance evaluation of a preclinical SPECT/CT system for multi-animal and multi-isotope

quantitative experiments. Sci Rep 2022; 12: 18161.
[30] Guo Z, Guillen DP, Grimm JR, Renteria C, Marsico C, Nikitin V and Arola D. High throughput automated characterization of enamel microstructure using synchrotron tomography and optical flow imaging. Acta Biomater 2024; 181: 263-271.
[31] Sacher SE, Hunt HB, Lekkala S, Lopez KA, Potts J, Heilbronner AK, Stein EM, Hernandez CJ and Donnelly E. Distributions of microdamage are altered between trabecular rods and plates in cancellous bone from men with type 2 diabetes mellitus. J Bone Miner Res 2022; 37: 740-752.
[32] Yu YE, Hu YJ, Zhou B, Wang J and Guo XE. Microstructure determines apparent-level mechanics despite tissue-level anisotropy and heterogeneity of individual plates and rods in normal human trabecular bone. J Bone Miner Res 2021; 36: 1796-1807.
[33] Li J, Zhang Z, Xie T, Song Z, Song Y and Zeng J. The preoperative Hounsfield unit value at the position of the future screw insertion is a better predictor of screw loosening than other methods. Eur Radiol 2023; 33: 1526-1536.
[34] Poilliot A, Gay-Dujak MH and Müller-Gerbl M. The quantification of 3D-trabecular architecture of the fourth cervical vertebra using CT osteoabsorptiometry and micro-CT. J Orthop Surg Res 2023; 18: 297.

Supplementary Table 1. Inter-observer consistency of CT bone microstructure parameters

Parameter	ICC (95% CI)	F-value	*P*-value
Volumetric BMD (HU)	0.884 (0.844-0.914)	16.249	<0.001
Bone volume fraction (%)	0.868 (0.823-0.902)	14.134	<0.001
Trabecular thickness (mm)	0.883 (0.842-0.913)	16.061	<0.001
Trabecular separation (mm)	0.881 (0.841-0.912)	15.857	<0.001
Trabecular number (1/mm)	0.854 (0.805-0.892)	12.713	<0.001
Cortical thickness (mm)	0.846 (0.794-0.885)	11.957	<0.001

Abbreviations: ICC, intraclass correlation coefficient; CI, confidence interval; BMD, bone mineral density; HU, Hounsfield Units; BV/TV, bone volume fraction; Tb.Th, trabecular thickness; Tb.Sp, trabecular separation; Tb.N, trabecular number; Ct.Th, cortical thickness.